Force/Moment Isotropy of 8/4-4 Parallel Six-Axis Force Sensor Based on Performance Atlases

Song Weishan, *Li Chenggang* *, *Wang Chunming*, *Song Yong*, *Wu Zefeng*, *Rajnathsing Hemant*

College of Mechanical and Electrical Engineering, Nanjing University of Aeronautics and Astronautics, Nanjing 210016, P. R. China

(Received 13 March 2018; revised 28 September 2018; accepted 5 December 2018)

Abstract: A six-axis force sensor with parallel 8/4-4 structure is introduced and its measurement principle is analyzed. Based on condition numbers of Jacobian matrix spectral norm of the sensor, the relationship between the force and moment isotropy and some structural parameters is deduced. Orthogonal test methods are used to determine the degree of primary and secondary factors that have significant effect on sensor characteristics. Furthermore, the relationship between each performance index and the structural parameters of the sensor is analyzed by the method of the atlas, which lays a foundation for structural optimization design of the force sensor.

Key words: six-axis force sensor; Jacobian matrix; condition number; isotropy; orthogonal test; indices atlases

CLC number: TN925 **Document code**: A **Article ID**: 1005-1120(2018)06-1018-09

0 Introduction

Six-axis force sensors can measure three-axis force and three-axis moment information in space at the same time and have widespread applications in various fields such as national defense science and technology[1], automotive electronics, robotics[2,3], automation[4] and machining[5].

From the elastomer material, six-axis force sensors can be divided into piezoelectric quartz crystal type[6], strain gauge type[7,8] and so on. From the overall structure of view, six-axis force sensors can be divided into Stewart-type parallel structure[9-11], cross beam structure[12-15], spoke type structure[8, 16] and so on. The isotropy of force and moment is the vital performance evaluation of six-axis force sensors[17]. The six-axis force transducer with a high isotropy of force and moment has the advantages of the same performance index and the same measurement accuracy in each direction. Masaru et al.[18] defined the isotropic evaluation index of a six-axis force sensor as the condition number of the Jacobian matrix spectral norm. Jin et al.[19] defined the translational stiffness and torsional stiffness of the sensor and analyzed the isotropy of the sensor in its solution space through the indices atlases. Yao et al.[17] put forward a kind of overall preloading six-axis force sensor, which can improve the dynamic stiffness of the sensor. Yao et al.[20] analyzed the forward and reverse isotropy of the six-branch Stewart six-axis force sensor by mathematical analysis method, and concluded that this sensor can't satisfy the requirement that both the reversed force and the reversed moment are isotropic at the same time. Tong et al.[21-23] described the Gough-Stewart parallel force sensor with single-leaf hyperboloid and composite single-leaf hyperboloid, and gave closed and analytic quasi-isotropic mathematical expressions on the premise of orthogonal characteristics. Jia, Li et al.[6,24] analyzed the isotropy of six-axis heavy force sensor, and combined the atlases analysis and genetic algorithm to optimize the structural

* Corresponding author, E-mail address: lichenggang@nuaa.edu.cn.

How to cite this article: Song Weishan, Li Chenggang, Wang Chunming, et al. Force/moment isotropy of 8/4-4 parallel six-axis force sensor based on performance atlases[J]. Trans. Nanjing Univ. Aero. Astro., 2018, 35(6): 1018-1026.
http://dx.doi.org/10.16356/j.1005-1120.2018.06.1018

parameters of the sensor. However the structural parameters of the spectrum analysis are less than those of all structural parameters, which makes structure optimization insufficient.

In this paper, an 8/4-4 structure parallel six-axis force sensor is introduced, and it has the advantage of achieving force and moment isotropy simultaneously by parameter optimization. Based on the principle of minimum number of condition numbers of the Jacobian matrix spectral norm, the isotropy of force and moment of the sensor is expressed. Through the numerical optimization method, the optimization of structural parameters of the force sensor under optimal isotropic performance is solved. Orthogonal experiments are used to determine the degree of primary and secondary factors that achieve a significant influence on the performance index of the sensor, and then the influence of structural parameters changes on the performance index of sensor is analyzed clearly by the method of spectrum optimization.

1 Measurement Principle of 8/4-4 Parallel Six-Axis Force Sensor

1.1 Mathematical model

The schematic diagram of the 8/4-4 six-axis force sensor is shown in Fig. 1. The upper and lower platforms are parallel to each other, and the eight branches are divided into two groups. The reference coordinate system $OXYZ$ is located on the geometric center of the upper platform, the Y-axis is vertically upward, the X-axis bisects $\angle b_1Ob_2$, and the Z-axis is determined based on the right hand rule. The coordinate system $O'X'Y'Z'$ is established at the geometric center of the lower platform, and its triaxial directions $X'Y'Z'$ are the same as those of the reference coordinate system. b_i stands for the center point of the flexible ball joints evenly distributed on the circumference of the upper platform, and B_i stands for the center point of the flexible ball joints on both concentric circles inner and outer the lower platform. Ignoring the mass of the branches and the friction between the flexible ball joints, the branches can be equivalent to two-force rod. In the structural parameters of the sensor, R_a represents the distribution radius of the center points of the flexible ball joints on the upper platform; R_{B1} and R_{B2} respectively represent the distribution radius of the center points of the flexible ball joints outer and inner of the lower platform; h represents the distance between the upper and lower platforms; α_1 and α_2 respectively represent the angle between Ob_1 and X-axis, and the angle between Ob_2 and X-axis; β_1 and β_2 respectively represent the angle between $O'B_1$ and X'-axis, and the angle between $O'B_2$ and X'-axis; θ_1 represents the angle between Ob_3 and $O'B_3$ in coordinate system $O'X'Y'Z'$. θ_2 represents the angle between Ob_4 and $O'B_4$ in the coordinate system $O'X'Y'Z'$.

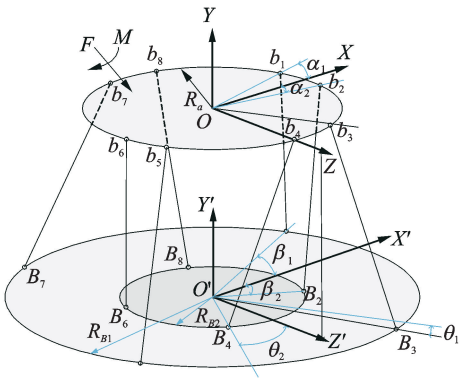

Fig. 1 Schematic diagram of 8/4-4 six-axis force sensor

Specifying the force and moment applied to the upper platform as F and M, the static balance equations for the upper platform can be expressed as

$$F=\sum_{i=1}^{8} f_i \cdot \frac{b_i-B_i}{|b_i-B_i|} \tag{1}$$

$$M=\sum_{i=1}^{8} f_i \cdot \frac{b_i\times(b_i-B_i)}{|b_i-B_i|}=\sum_{i=1}^{8} f_i \cdot \frac{B_i\times b_i}{|b_i-B_i|} \tag{2}$$

Eqs. (1) and (2) can be rewritten in the form of a matrix, which is

$$\boldsymbol{F}_W=\boldsymbol{J}\cdot\boldsymbol{f} \tag{3}$$

where

$$\boldsymbol{F}_W=[\boldsymbol{F}\quad\boldsymbol{M}]^{\mathrm{T}}$$

$$\boldsymbol{f}=[f_1\quad f_2\quad f_3\quad f_4\quad f_5\quad f_6\quad f_7\quad f_8]^{\mathrm{T}}$$

Jacobian matrix $\boldsymbol{J}$ is shown as

$$\boldsymbol{J}=\begin{bmatrix}\dfrac{b_1-B_1}{|b_1-B_1|} & \dfrac{b_2-B_2}{|b_2-B_2|} & \cdots & \dfrac{b_8-B_8}{|b_8-B_8|}\\ \dfrac{B_1\times b_1}{|b_1-B_1|} & \dfrac{B_2\times b_2}{|b_2-B_2|} & \cdots & \dfrac{B_8\times b_8}{|b_8-B_8|}\end{bmatrix} \tag{4}$$

1.2 Isotropic indicators of force and moment

Isotropy of force and moment is an important performance evaluation index of six-axis force sensors. The Jacobian matrix $\boldsymbol{J}$ can be expressed in the form of $[\boldsymbol{J}_F \quad \boldsymbol{J}_M]^T$ because of different dimensions of the first three lines and the last three lines. From Eq. (3), we know that the smaller the condition number of Jacobian matrix $\boldsymbol{J}$ is, the better the numerical stability could be. The smaller the influence of the small change of $\boldsymbol{f}$ on the $\boldsymbol{F}_W$ is, the less influence of various errors in all directions on the measurement result can get. The better the force transmission performance of the sensor is, that is, physical properties of the sensor tend to be consistent in all directions, the better the isotropic degree of force and moment will be.

According to the minimum principle of conditional number of Jacobian matrix spectral norm, the isotropic degrees of force and moment μ_F and μ_M are expressed respectively as the reciprocal of the conditional number of Jacobian matrix of force and moment, i. e.

$$\mu_F=\frac{1}{\mathrm{cond}(\boldsymbol{J}_F)},\quad \mu_M=\frac{1}{\mathrm{cond}(\boldsymbol{J}_M)} \tag{5}$$

In order to make the sensor isotropic, the sensor should be structural symmetric, the isotropic degree of force and moment is 1, and the condition number of Jacobian matrix is also 1 at this moment. That is, $\mathrm{cond}(\boldsymbol{J}_F)=\mathrm{cond}(\boldsymbol{J}_M)=1$. $\boldsymbol{J}\boldsymbol{J}^T$ must be a generally diagonal matrix, which can be expressed as

$$\boldsymbol{J}\boldsymbol{J}^T=\begin{bmatrix}\boldsymbol{J}_F\boldsymbol{J}_F^T & \boldsymbol{J}_F\boldsymbol{J}_M^T\\ \boldsymbol{J}_M\boldsymbol{J}_F^T & \boldsymbol{J}_M\boldsymbol{J}_M^T\end{bmatrix} \tag{6}$$

where $\boldsymbol{J}_F\boldsymbol{J}_F^T$ and $\boldsymbol{J}_M\boldsymbol{J}_M^T$ should be diagonal matrices, and $\boldsymbol{J}_F\boldsymbol{J}_M^T$ and $\boldsymbol{J}_M\boldsymbol{J}_F^T$ should be zero matrices of 3×3. They can be expressed as

$$\begin{cases}\boldsymbol{J}_F\boldsymbol{J}_F^T=\mathrm{diag}(\gamma_{F1},\gamma_{F2},\gamma_{F3})/L^2\\ \boldsymbol{J}_M\boldsymbol{J}_M^T=\mathrm{diag}(\gamma_{M1},\gamma_{M2},\gamma_{M3})/L^2\end{cases} \tag{7}$$

$$\boldsymbol{J}_F\boldsymbol{J}_M^T=\boldsymbol{J}_M\boldsymbol{J}_F^T=\boldsymbol{O} \tag{8}$$

When $\gamma_{F1}=\gamma_{F2}=\gamma_{F3}$, $\gamma_{M1}=\gamma_{M2}=\gamma_{M3}$, the sensor satisfies the force and moment isotropy. At this moment, both condition numbers of $\boldsymbol{J}_F$ and $\boldsymbol{J}_M$ are equal to 1.

Simplifying $\boldsymbol{J}\boldsymbol{J}^T$ as

$$\boldsymbol{J}\boldsymbol{J}^T=\begin{bmatrix}\gamma_{F1} & 0 & 0 & X_1 & X_2 & 0\\ 0 & \gamma_{F2} & 0 & -X_2 & X_1 & 0\\ 0 & 0 & \gamma_{F3} & 0 & 0 & -2X_1\\ X_1 & -X_2 & 0 & \gamma_{M1} & 0 & 0\\ X_2 & X_1 & 0 & 0 & \gamma_{M2} & 0\\ 0 & 0 & -2X_1 & 0 & 0 & \gamma_{M3}\end{bmatrix}\cdot\frac{1}{L^2} \tag{9}$$

where

$L=(R_{B1}^2+R_a^2-2R_{B1}R_a\cos\theta_1+h^2)^{1/2}=(R_{B2}^2+R_a^2-2R_{B2}R_a\cos\theta_2+h^2)^{1/2}$, $\theta_1=\alpha_i-\beta_i$ $(i=1,3,5,7)$, $\theta_2=\alpha_i-\beta_i$ $(i=2,4,6,8)$, $\gamma_{F1}=\gamma_{F3}=2(R_{B1}^2+R_{B2}^2+2R_a^2)-4R_a(R_{B1}\cos\theta_1+R_{B2}\cos\theta_2)$, $\gamma_{F2}=8h^2$, $\gamma_{M1}=\gamma_{M3}=4R_a^2h^2$, $\gamma_{M2}=4R_a^2(R_{B1}^2\sin\theta_1^2+R_{B2}^2\sin\theta_2^2)$, $X_1=-2R_ah(R_{B1}\sin\theta_1+R_{B2}\sin\theta_2)$, $X_2=2R_ah(R_{B1}\cos\theta_1+R_{B2}\cos\theta_2-2R_a^2)$.

From $X_1=X_2=0$, R_{B1} and R_{B2} can be respectively expressed as

$$\begin{aligned}R_{B1}&=-\frac{2R_a\sin\theta_2}{\sin(\theta_1-\theta_2)}\\ R_{B2}&=-\frac{2R_a\sin\theta_1}{\sin(\theta_1-\theta_2)}\end{aligned} \tag{10}$$

Substituting R_{B1} and R_{B2} into $\gamma_{M1}-\gamma_{M2}=0$, we can obtain

$$\frac{8R_a^2\sin^2\theta_1\sin^2\theta_2}{\sin^2(\theta_1-\theta_2)}-h^2=0 \tag{11}$$

Thus, h can be expressed as

$$h=\frac{2\sqrt{2}R_a\sin\theta_1\sin\theta_2}{\sin(\theta_1-\theta_2)} \tag{12}$$

Substituting R_{B1}, R_{B2} and h into $\gamma_{F1}-\gamma_{F2}=0$, we can obtain

$$\frac{7\cos2\theta_1\cos2\theta_2-6\cos2\theta_1-6\cos2\theta_2-\sin2\theta_1\cos2\theta_2+5}{\cos(2\theta_1-2\theta_2)-1}=0 \tag{13}$$

In Eq. (13), $\cos(2\theta_1-2\theta_2)-1\neq0$, that is, $\theta_1\neq\theta_2$.

It can be seen that, given the range of R_a and θ_2, Eq. (13) can be solved by the numerical method, and θ_1, R_a and θ_2 can be brought into the expression of R_{B1}, R_{B2} and h. Thus all structural pa-

rameters of the sensor meeting the force and moment isotropic can be gained.

2 Determination of Main Relation of Each Parameter Based on Orthogonal Experiment

From Eqs. (5-9), it can be seen that the force and moment isotropy of the sensor are related to multiple factors of the sensor, including R_a, R_{B1}, R_{B2}, h, θ_1 and θ_2. In order to study the degree of primary and secondary factors that have a significant influence on the sensor characteristics, the method of orthogonal experiment[25,26] is used in combination with the experiment.

2.1 Orthogonal design

The orthogonal experiment includes six factors, which are R_a, R_{B1}, R_{B2}, h, θ_1 and θ_2, respectively. The last blank column is left as the error column. Four levels are selected in each factor[27]. According to the limited physical size of the sensor, the level parameter settings of the orthogonal test are shown in Table 1.

Table of $L_{32}(4^7)$ is selected for orthogonal experiment design. Tables 2 and 3 give only the first six experimental data. The combination of structural parameters for each test case is expressed in terms of levels. There are four levels for each factor, and each level appears eight times in 32 trials.

Table 1 Orthogonal factor level table

Level	R_a (A)	R_{B1} (B)	R_{B2} (C)	h (D)	θ_1 (E)	θ_2 (F)	
1	0.09	0.12	0.03	0.02	−3	20	1
2	0.10	0.13	0.04	0.03	−5	24	2
3	0.11	0.14	0.05	0.04	−7	28	3
4	0.12	0.15	0.06	0.05	−9	32	4

2.2 Analysis of orthogonal experiment results

Intuitive analysis is used to compare the range $\dot{R}$ of average values of the four levels for each factor, then the order of primary and secondary of importance for six factors is determined.

In this example, within the given range of each factor level, R_a (factor A), R_{B1} (factor B), R_{B2} (factor C), h (factor D), θ_1 (factor E) and θ_2 (factor F), the order of the six factors that influence the force isotropic μ_F can be arranged(primary→secondary): D,A,E,B,F,C. Using the same method to make orthogonal experiment on μ_M, the main and secondary order of factors that influence the moment isotropic μ_M can be arranged (primary→secondary): D,E,B,C,F,A.

Since the factor A is limited strictly in practice and cannot be changed within a wide range, it has a weak influence even though it ranked in front on μ_F. From the above analysis, it is found that the influence of factors B, D and E (the corresponding structural parameters of R_{B1}, h and θ_1) on μ_F, μ_M is the most significant.

Table 2 Orthogonal experiment designs table of μ_F

Test number	A 1	B 2	C 3	D 4	E 5	F 6	7	Data of μ_F
1	2	2	2	4	1	3	2	0.650 687
2	1	3	4	2	1	4	3	0.842 184
3	4	2	1	3	2	4	1	0.687 600
4	4	1	3	3	3	3	3	0.649 931
5	3	4	2	3	4	4	3	0.978 875
6	2	4	4	1	2	2	1	0.551 972
…	…	…	…	…	…	…	…	…
$\bar{\mathrm{I}}$	0.748	0.72	0.778	0.675	0.79	0.757		
$\bar{\mathrm{II}}$	0.761	0.75	0.739	0.857	0.714	0.725		
$\bar{\mathrm{III}}$	0.713	0.772	0.758	0.813	0.721	0.775	Primary → Secondary:	
$\bar{\mathrm{IV}}$	0.797	0.776	0.742	0.673	0.793	0.761	D,A,E,B,F,C	
Range $\hat{R}$	0.084	0.056	0.039	0.184	0.079	0.050		

Table 3 Orthogonal experiment design table of μ_M

Test number	A 1	B 2	C 3	D 4	E 5	F 6	7	Data of μ_M
1	2	2	2	4	1	3	2	0.342 693
2	1	3	4	2	1	4	3	0.919 836
3	4	2	1	3	2	4	1	0.427 649
4	4	1	3	3	3	3	3	0.588 236
5	3	4	2	3	4	4	3	0.805 207
6	2	4	4	1	2	2	1	0.723 176
…	…	…	…	…	…	…	…	…
$\bar{\mathrm{I}}$	0.664	0.566	0.580	0.731	0.529	0.599		
$\bar{\mathrm{II}}$	0.655	0.589	0.631	0.770	0.578	0.611		
$\bar{\mathrm{III}}$	0.656	0.752	0.651	0.593	0.700	0.647	Primary → Secondary:	
$\bar{\mathrm{IV}}$	0.590	0.658	0.702	0.471	0.759	0.707	D,E,B,C,F,A	
Range $\hat{R}$	0.074	0.186	0.122	0.299	0.230	0.108		

Performance atlases from the overall point of view more vividly show the distribution of the various structural parameters of the sensor on the performance index. Therefore, with the help of space model theory[26], some atlases of the variation of the sensor's performance index with structural parameters (R_{B1}, h and θ_1) are plotted on the plane in Section 3.

3 Performance Atlases

Let $R_{B2} = P_d \cdot R_{B1}$ (P_d is a constant, and specified to be 0.38 as an example), the parameter ranges are limited to 0.1m$<R_{B1}<$0.2 m, 0$<h<$0.15 m, $-45° < \theta_1 < 45°$. According to Eq. (5), plots of sensor performance indices μ_F, μ_M with three main structural parameters R_{B1}, h, θ_1 are plotted when $\theta_2-\theta_1=20°$, $\theta_2-\theta_1=40°$ and $\theta_2-\theta_1=50°$ ($\theta_2-\theta_1$ is the difference of positioning angle), as shown in Figs. 2—10. It is found that the trend presented by the atlas does not change with the change of $\theta_2-\theta_1$. Figs. 4, 7 and 10 are comprehensive atlases of μ_F and μ_M respectively. The areas marked by bright color represent the excellent isotropy of force and moment.

Based on the analysis of the performance atlases, we can get the following results:

(1) When the sensor height needs to be as small as possible, a smaller $\theta_2-\theta_1$ can be taken.

(2) Sensor structure parameters should be designed by selecting areas where the contour changes are relatively flat.

(3) For force isotropic design, $\theta<20°$ and $R_{B1}<0.16$ m should be selected and $\theta_2-\theta_1$ should be increased moderately. The bright color region broadens, making the optional parameter range of the sensor larger. For moment isotropic design, θ_1 can be chosen between $-9°$ and $-45°$, and R_{B1} can be chosen between 0.12 m and 0.14 m. If R_{B1} needs to be smaller, $\theta_2-\theta_1$ can be increased appropriately.

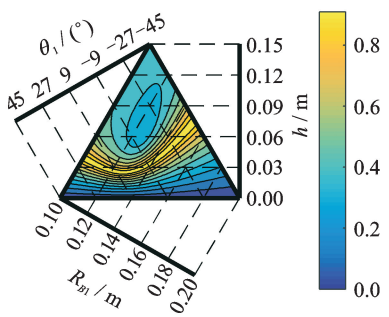

Fig. 2 Force isotropic atlas μ_F ($\theta_2-\theta_1=20°$)

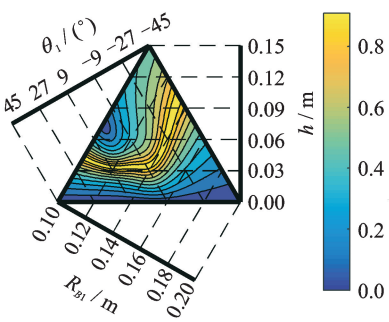

Fig. 3 Moment isotropic atlas μ_M ($\theta_2-\theta_1=20°$)

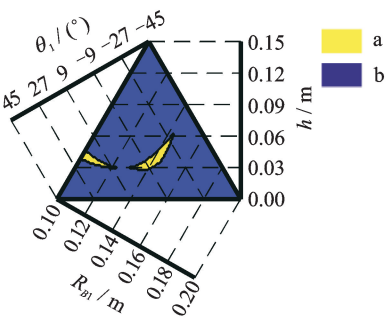

Fig. 4 Comprehensive atlas of μ_F and μ_M ($\theta_2-\theta_1=20°$)

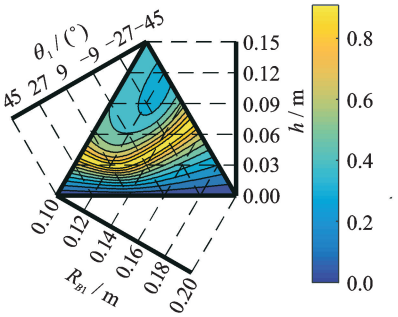

Fig. 5 Force isotropic atlas μ_F ($\theta_2-\theta_1=40°$)

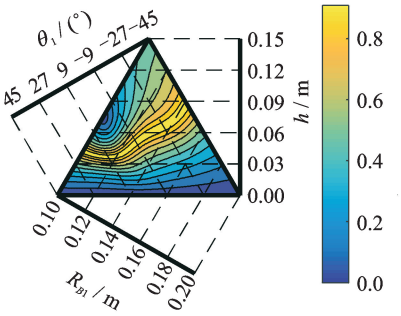

Fig. 6 Moment isotropic atlas μ_M ($\theta_2-\theta_1=40°$)

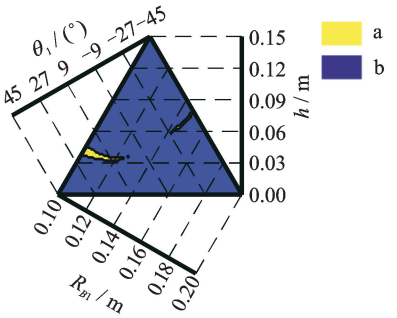

Fig. 7 Comprehensive atlas of μ_F and μ_M ($\theta_2-\theta_1=40°$)

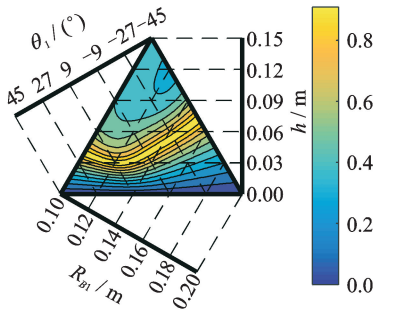

Fig. 8 Force isotropic atlas μ_F ($\theta_2-\theta_1=50°$)

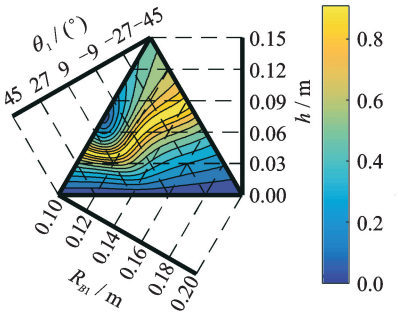

Fig. 9 Moment isotropic atlas μ_M ($\theta_2-\theta_1=50°$)

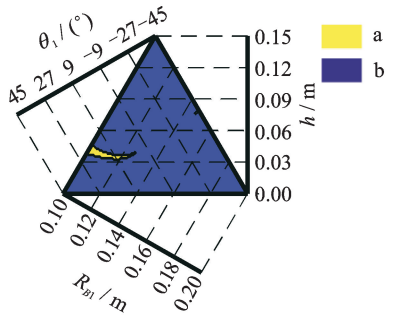

Fig. 10 Comprehensive atlas of μ_F and μ_M ($\theta_2-\theta_1=50°$)

(4) Aiming at the higher design requirements of force and moment isotropy, the structure parameter selection should be in the region "a" shown in Figs. 4, 7 and 10. The isotropy of the force and moment in region "a" is greater than 0.8, and that in region "b" is not greater than 0.8.

4 Simulation Verification

According to the optimization method mentioned in Section 3, by combining the orthogonal experiment analysis and the performance atlases as shown in Fig. 11, a set of sensor structural parameters with excellent force and moment isotropy is selected as follows.

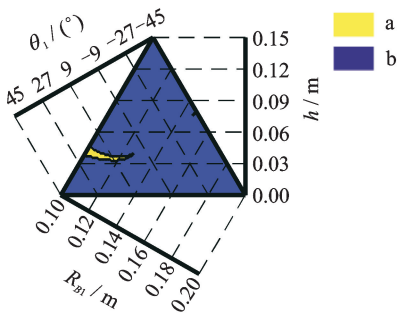

Fig. 11 Comprehensive atlas of μ_F and μ_M ($\theta_2-\theta_1=31°$)

$$R_a=0.1\text{m};R_{B1}=0.15\text{m};R_{B2}=0.057\text{m};$$
$$h=0.04\text{m};\theta_1=-11°;\theta_2=20° \quad (14)$$

Bringing these structural parameters into the theoretical model of Section 1, the force and moment isotropy of the sensor are calculated as

$$\mu_F=0.998\ 7,\mu_M=0.990\ 2 \quad (15)$$

The load range of the sensor is $F_x=F_y=F_z=1$ kN and $M_x=M_y=M_z=100$ Nm. Replacing each branch of the sensor with a spring, a virtual prototype of the 8/4-4 parallel six-axis force sensor is built in automatic dynamic analysis of mechanical systems(ADAMS). Now the lower platform of the sensor is fixed, and the generalized six-axis force in each direction is applied to the center point of the upper platform. Each force component is loaded successively from small to large. After reaching the maximum value, it is unloaded from large to small, and the eight branching forces of the sensor in the ADAMS simulation are recorded. According to the method in Ref. [28], the calibration matrix $\boldsymbol{G}_a$ can be calculated as

$$\boldsymbol{G}_a = \begin{bmatrix} -0.476 & 0.738\ 1 & -0.662\ 4 & 0.345\ 8 & 0.475\ 6 & -0.738\ 7 & 0.661\ 9 & -0.346\ 1 \\ 0.580\ 8 & 0.579\ 0 & 0.578\ 3 & 0.576\ 9 & 0.578\ 6 & 0.577\ 7 & 0.578\ 3 & 0.579\ 7 \\ 0.662\ 9 & -0.345\ 1 & -0.475\ 1 & 0.739\ 0 & -0.661\ 5 & 0.346\ 7 & 0.476\ 5 & -0.737\ 8 \\ 0.023\ 6 & -0.005\ 0 & -0.052\ 9 & -0.057\ 6 & -0.023\ 5 & 0.005\ 1 & 0.053\ 0 & 0.057\ 7 \\ -0.041\ 0 & 0.040\ 9 & -0.041\ 0 & 0.040\ 9 & -0.041\ 0 & 0.040\ 9 & -0.041\ 0 & 0.040\ 9 \\ 0.053\ 0 & 0.057\ 7 & 0.023\ 6 & -0.005\ 0 & -0.052\ 9 & -0.057\ 6 & -0.023\ 5 & 0.005\ 1 \end{bmatrix}^{\mathrm{T}} \tag{16}$$

According to Eq. (5), the force and moment isotropy of the six-axis force sensor obtained by ADAMS simulation can be calculated as

$$\mu_{Fa} = 0.996\ 2, \mu_{Ma} = 0.999\ 7 \tag{17}$$

It can be seen from the comparison between Eq. (15) and Eq. (17) that the isotropic degrees of force and moment calculated according to the simulation and the theoretical model are very approximate. The mathematical model and the force and torque isotropic optimization algorithm of the 8/4-4 parallel six-axis force sensor are proved to be correct and accurate.

5 Conclusions

In this paper, the isotropic properties of force and moment are analyzed based on 8/4-4 parallel six-axis force sensor. A mathematical model of 8/4-4 parallel six-axis force sensor is established. Based on the definition of each performance index of sensor, the numerical optimization method is used to select the combination of six-axis force sensor structure parameters that meet the requirements of performance index. Through orthogonal experiment, the primary and secondary influences of each structural parameter on the six performance indexes are analyzed, and then the performance model is drawn and analyzed by using the spatial model theory. From the performance atlases of sensor, the regularity between the isotropy of the force and moment and the structural parameters of the sensor is analyzed, which lays a good foundation for the reasonable selection of the sensor parameters with the expected performance. The accuracy of mathematical model and optimization algorithm of the 8/4-4 parallel six-axis force sensor are confirmed by ADAMS simulation. The conclusions based on the performance atlas can be summarized as follows:

(1) The general trend of the isotropic curve is that the smaller $\theta_2 - \theta_1$ is, the smaller the distance between two platforms can get when the force and the moment reach isotropy.

(2) When $\theta_2 - \theta_1$ is large, h is between 0.03 m and 0.05 m, and the contour is relatively flat, which shows that the slight change of structural parameters in this area has little effect on the performance index. Designing in this area allows a slightly larger tolerance to structural parameters and helps to reduce processing and assembly costs.

(3) When the force reaches isotropy, the distance between two platforms increases generally, which is in favor of sensor processing. When the moment reaches isotropy, R_{B1} generally shows a decreasing trend, which is beneficial to make the sensor compact.

Acknowledgements

This work was supported by the Open Foundation of Graduate Innovation Base (Laboratory) of Nanjing University of Aeronautics and Astronautics (No. kfjj20170512) and the National Natural Science Foundation of China (No. 51175263).

References:

[1] WU Y, YU K, JIAO J, et al. Dynamic isotropy design and analysis of a six-DOF active micro-vibration isolation manipulator on satellites[J]. Robotics and Computer-Integrated Manufacturing, 2018, 49: 408-425.

[2] KIM U, LEE D H, YONG B K, et al. A novel six-axis force/torque sensor for robotic applications[J]. IEEE/ASME Transactions on Mechatronics, 2017, 22(3): 1381-1391.

[3] CHAVEZ F J A, TRAVERSARO S, PUCCI D, et al. Model based in situ calibration of six axis force torque sensors [C]// IEEE-Ras, International Con-

ference on Humanoid Robots. Cancun, Mexico: IEEE, 2017:422-427.

[4] ZHANG T, LIU H, JIANG L, et al. Development of a flexible 3-D tactile sensor system for anthropomorphic artificial hand[J]. IEEE Sensors Journal, 2013, 13(2): 510-518.

[5] YAO Y, WU H. Force Jacobianan matrix for 3-DOF cable-driven mechanism with rotation in wind tunnel [J]. Journal of Nanjing University of Aeronautics & Astronautics, 2011, 43(1): 75-78. (in Chinese)

[6] LI Y J, WANG G C, ZHAO D, et al. Research on a novel parallel spoke piezoelectric 6-DOF heavy force/torque sensor[J]. Mechanical Systems & Signal Processing, 2013, 36(1): 152-167.

[7] ZHAO Y, ZHANG C, ZHANG D, et al. Mathematical model and calibration experiment of a large measurement range flexible joints 6-UPUR six-axis force sensor[J]. Sensors (Basel), 2016, 16(8): 1271.

[8] YAO J, ZHANG H, XIANG X, et al. A 3-D printed redundant six-component force sensor with eight parallel limbs[J]. Sensors and Actuators A: Physical, 2016, 247: 90-97.

[9] YAO J, CAI D, ZHANG H, et al. Task-oriented design method and research on force compliant experiment of six-axis wrist force sensor[J]. Mechatronics, 2016, 35: 109-121.

[10] ESTEVEZA P, BANKA J M, PORTAA M, et al. 6 DOF force and torque sensor for micro-manipulation applications[J]. Sensors and Actuators A: Physical, 2012,186:86-93.

[11] YAO J, HOU Y, WANG H, et al. Spatially isotropic configuration of Stewart platform-based force sensor[J]. Mechanism and Machine Theory, 2011, 46(2): 142-155.

[12] WANG Y, ZUO G, CHEN X, et al. Strain analysis of six-axis force/torque sensors based on analytical method[J]. IEEE Sensors Journal, 2017, 17(14): 4394-4404.

[13] YUAN C, LUO L P, YUAN Q, et al. Development and evaluation of a compact 6-axis force/moment sensor with a serial structure for the humanoid robot foot[J]. Measurement, 2015, 70: 110-122.

[14] CHEN D, SONG A, LI A. Design and calibration of a six-axis force/torque sensor with large measurement range used for the space manipulator[J]. Procedia Engineering, 2015, 99: 1164-1170.

[15] SUN Y, LIU Y, JIN M, et al. Design and optimization of a novel six-axis force/torque sensor with good isotropy and high sensitivity[C]//IEEE International Conference on Robotics and Biomimetics. Shenzhen, China: IEEE, 2013:631-638.

[16] YAO J, WANG D, CAI D, et al. Fault-tolerant strategy and experimental study on compliance assembly of a redundant parallel six-component force sensor [J]. Sensors and Actuators A: Physical, 2018,272: 114-124.

[17] YAO J, ZHANG H, ZHU J, et al. Isotropy analysis of redundant parallel six-axis force sensor[J]. Mechanism and Machine Theory, 2015, 91: 135-150.

[18] MASARU U, YOSHIHIRO N, KYOJIRO H, et al. Evaluation of the robot force sensor structure using singular value decomposition[J]. Advanced Robotics, 2010,5(1): 39-52.

[19] JIN Z, GAO F, ZHANG X. Design and analysis of a novel isotropic six-component force/torque sensor [J]. Sensors & Actuators A Physical, 2003, 109(1-2): 17-20.

[20] YAO J, WANG D, LIN X, et al. Isotropy analysis of a stiffness decoupling 8/4-4 parallel force sensing mechanism[C]// International Conference on Intelligent Robotics and Applications. Cham: Springer, 2017:87-97.

[21] TONG Z, JIANG H, JINGFENG H E, et al. Optimal design of acceleration sensor based on generalized gough-stewart parallel manipulator lying on pair of circular hyperboloids[J]. Journal of Mechanical Engineering, 2014, 50(13): 35.

[22] TONG Z, HE J, JIANG H, et al. Optimal design of a class of generalized symmetric gough-stewart parallel manipulators with dynamic isotropy and singularity-free workspace[J]. Robotica, 2012, 30(2): 305-314.

[23] HE J F, JIANG H Z, TONG Z Z, et al. Study on dynamic isotropy of a class of symmetric spatial parallel mechanisms with actuation redundancy [J]. Journal of Vibration & Control, 2012, 18(8): 1156-1164.

[24] JIA Z, ZHU H, LIU W, et al. Performance analysis and structure optimization of six-axis heavy force sensor based on Stewart platform[J]. Chinese Journal of Scientific Instrument, 2010, 31(2):341-346. (in Chinese)

[25] GUO A, ZHAO J, LI J, et al. Forming parameters optimisation of biomass cushion packaging material by orthogonal test[J]. Materials Research Innovations, 2016, 19(sup5): S5-521-S5-525.

[26] LIU Y, SUN Y, INFIELD D, et al. A hybrid fore-

casting method for wind power ramp based on orthogonal test and support vector machine (OT-SVM) [J]. IEEE Transactions on Sustainable Energy, 2016, PP(99): 1-1.

[27] YU H Z. Industrial experimental design technology [M]. Nanjing: Southeast University Press, 1990.

[28] YU H, JIANG J, XIE L, et al. Design and static calibration of a six-dimensional force/torque sensor for minimally invasive surgery[J]. Minimally Invasive Therapy, 2014, 23(3): 136-143.

Ms. **Song Weishan** received her B. S. degree in Mechanical Engineering and Automation from Nanjing University of Aeronautics and Astronautics(NUAA) in 2016. She is currently a postgraduate student in Mechanical and Electrical Engineering of NUAA. Her research interests focus on mechanics and electronics, especially structure design and analytic modeling for force sensor.

Dr. **Li Chenggang** received his B. S. degree in Hydraulic Transmission and Control from Jilin University of Technology in 1998. He received his M. S. and Ph. D. degrees in Mechanical and Electrical Engineering from Jilin University in 2001 and Beijing Institute of Technology in 2004, respectively. He is currently an associate professor in NUAA. His major research interests include system design and industrial robot, tissue modeling and contact analysis, multidimensional sensor design, and parallel mechanism.

Mr. **Wang Chunming** received his B. S. degree in Mechanical Engineering and Automation from NUAA in 2016. He is currently a postgraduate student in Mechanical and Electrical Engineering of NUAA. His research interests include robot design, modeling and control, flexible joint and physical human-robot interaction.

Mr. **Song Yong** received his B. S. degree in Mechanical and Electrical Engineering from Nanjing Agricultural University in 2017. He is currently a postgraduate student in Mechanical and Electrical Engineering of NUAA. His current research interests include industrial robot and analytic modeling for tactile sensor.

Mr. **Wu Zefeng** received his B. S. degree in Mechanical Design Manufacture and Automation from Nanchang Hangkong University in 2017. He is currently a postgraduate student in Mechanical and Electrical Engineering of NUAA. His current research interests focus on mechanics and electronics.

Mr. **Rajnathsing Hemant** received his B. S. degree in Mechatronics Engineering from the University of Mauritius in 2014. He is currently a postgraduate student in Mechanical and Electrical Engineering of NUAA. His research interests include machine vision and human-robot collaboration safety.

(Production Editor: Wang Jing)